Electronic Supplementary Material (ESI) for Dalton Transactions.

Supporting Information

Static and dynamic coordination behaviours of copper(I) ions in hexa(2-pyridyl)benzene ligand systems

Hyunchul Kwon[a] and Eunsung Lee*[a,b,c]

[a] Department of Chemistry, Pohang University of Science and Technology, 77 Cheongam-Ro, 37673, Pohang, Republic of Korea.

[b] Center for Self–assembly and Complexity, Institute for Basic Science (IBS), 77 Cheongam-Ro, 37673, Pohang, Republic of Korea.

[c] Division of Advanced Materials Science, Pohang University of Science and Technology, 77 Cheongam-Ro, 37673, Pohang, Republic of Korea.

*E-mail: eslee@postech.ac.kr

Table of Contents

1. General Information

Chemical reagents. 2-phenylpyridine, triphenylphosphine, potassium carbonate, 2-bromopyridine, 2-bromo-5-methylpyridine, copper(I) chloride and triethylamine were purchased from commercial sources and used as received without further purification. 5-methyl-2-phenylpyridine[1] and $[(\eta^6\text{-}C_6H_6)RuCl_2]_2$[2] was synthesized following the procedure described in reference. *N*-methyl-2-pyrrolidone (NMP) was dried by molecular sieves (3 Å) prior to use. Tetrahydrofuran (THF) was distilled over sodium benzophenone and stored in molecular sieves (3 Å) prior to use. Acetonitrile and d_3-acetonitrile were distilled over P_2O_5 and stored in molecular sieves (4 Å) prior to use.

Experiment equipment. Nuclear magnetic resonance (NMR) spectra were recorded on a Bruker DRX spectrometer operating at 500 MHz and 125 MHz for ^{1}H and ^{13}C acquisitions, respectively. Elemental analysis (EA) for C, H, and N were conducted using Truspec Micro (Leco). Single crystal X-ray diffraction (SC-XRD) data were collected on a Bruker D8 VENTURE diffractometer equipped with graphite monochromated Mo Kα radiation (λ = 0.71073 Å) and Cu K α radiation (λ = 1.54178 Å) or synchrotron radiation of 2D-SMC at the Pohang Accelerator Laboratory (PAL, Korea) using an ADSC Quantum-210 detector furnished with a silicon (111) double crystal monochromator (DCM) at 100 K.

X-Ray Crystallography. Using Olex[3], the structure was solved by ShelXT[4] using Intrinsic Phasing and refined by ShelXTL[5] using Least Squares minimization. Crystal data and experimental details are listed in **Table 1**.

Sample Preparation for ^{1}H VT NMR and 2D EXSY Experiment of 2a. A saturated solution of complex **2a** was prepared by stirring 2.0 mg of the complex in 1 mL of CD_3CN and filtered. The solution was loaded in a screw-cap NMR tube.

Sample Preparation for ^{1}H VT NMR and 2D EXSY Experiment of 1 and 2b. The nmr sample of **1** was prepared by loading 1.0 mg of complex **1** with 500 μL of CD_3CN in a screw-cap NMR tube. The NMR sample of **2b** was prepared by loading 1.0 mg of complex **1** with 500 μL of CD_3CN in a screw-cap NMR tube.

2. PXRD data

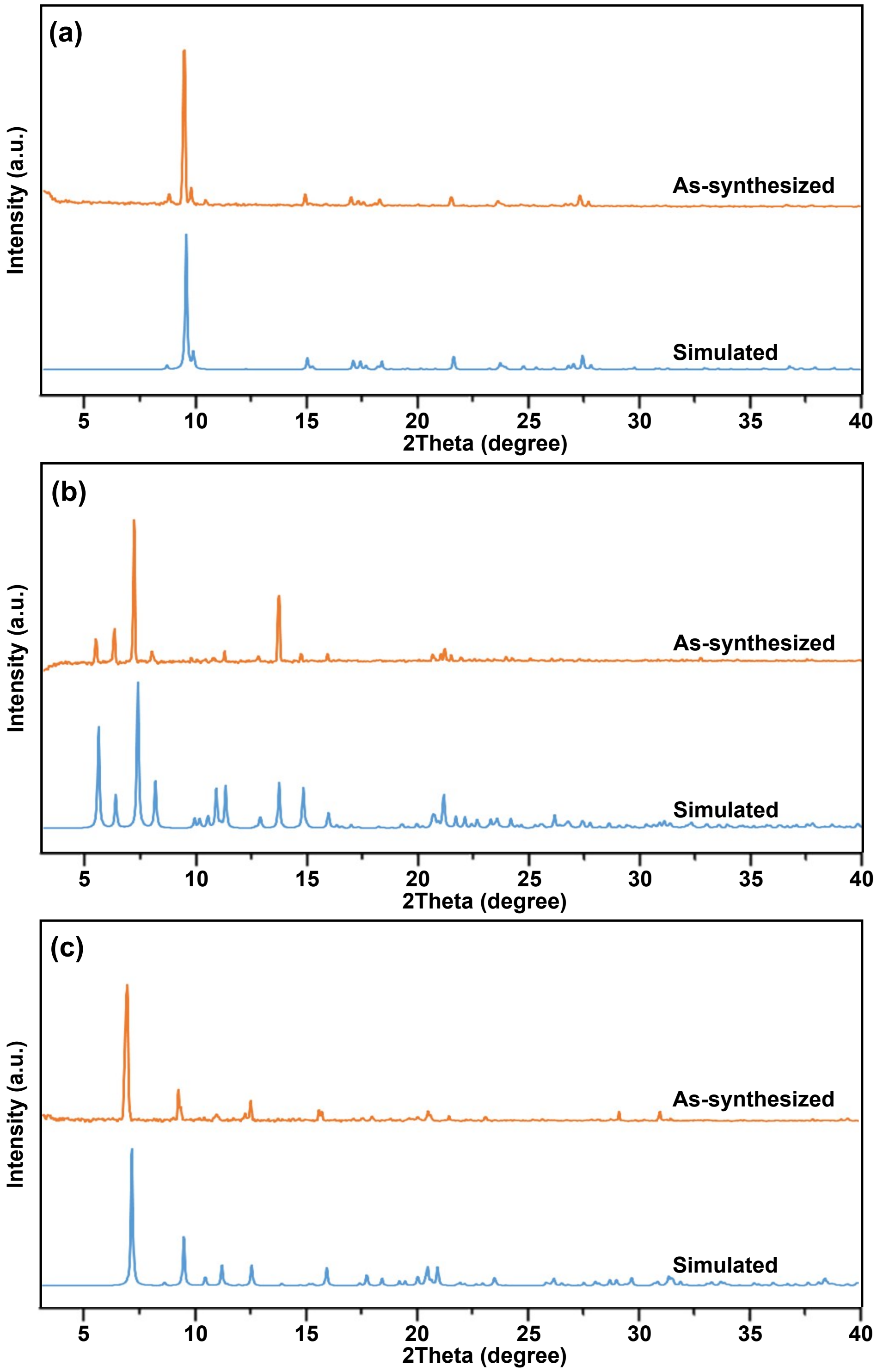

Figure S1. PXRD patterns of $[L_HCu_4Cl_4]_n$ (**3**) (a), $[L_MCu_4Cl_4(CH_3CN)]_n$ (**4**) (b) and $[L_MCu_4Cl_4\cdot THF]_n$ (**5**) (c).

3. NMR data

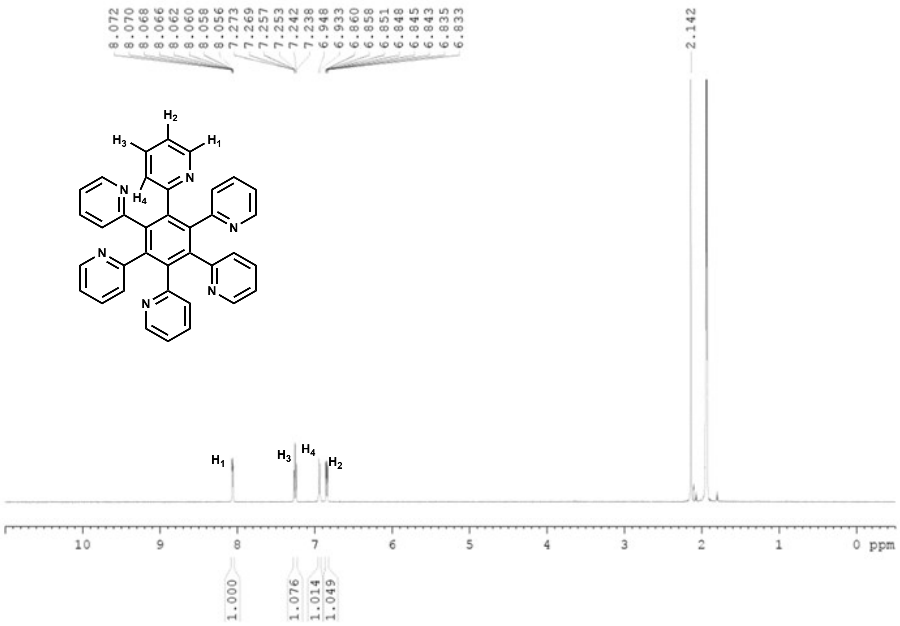

Figure S2. ^{1}H NMR spectrum of hexa(2-pyridyl)benzene (**L_H**) in CD_3CN.

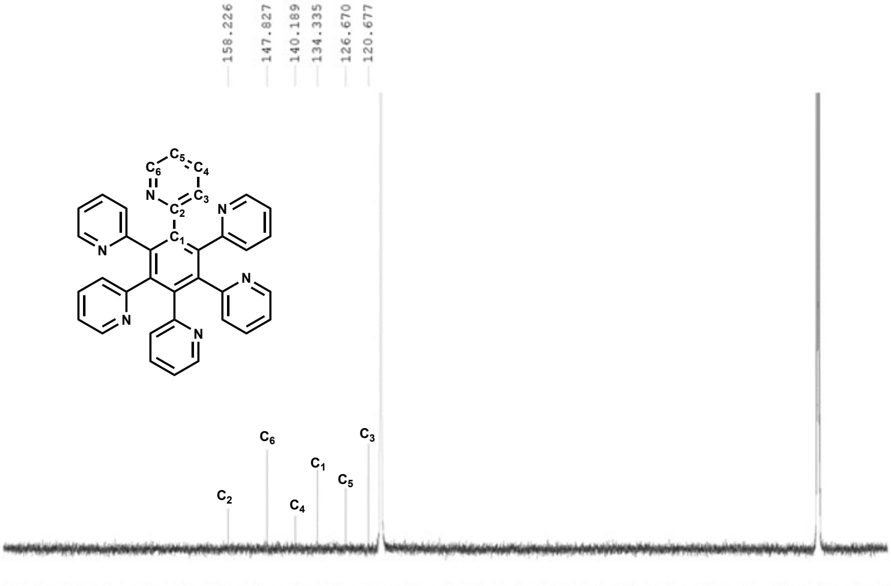

Figure S3. ^{13}C NMR spectrum of hexa(2-pyridyl)benzene (**L_H**) in CD_3CN.

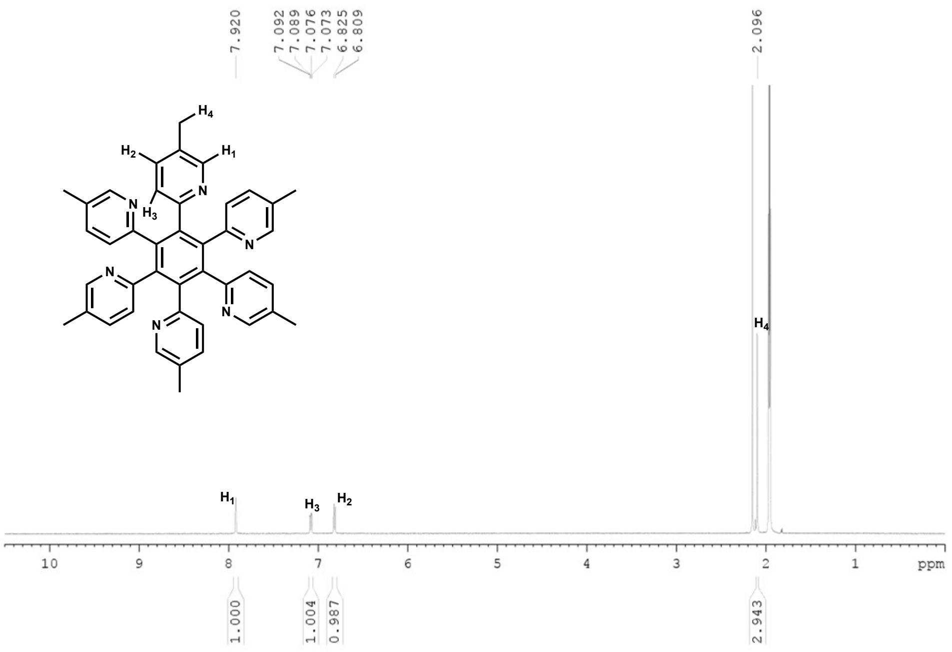

Figure S4. ^{1}H NMR spectrum of hexa(2-(5-methylpyridyl))benzene ($\mathbf{L_M}$) in CD_3CN.

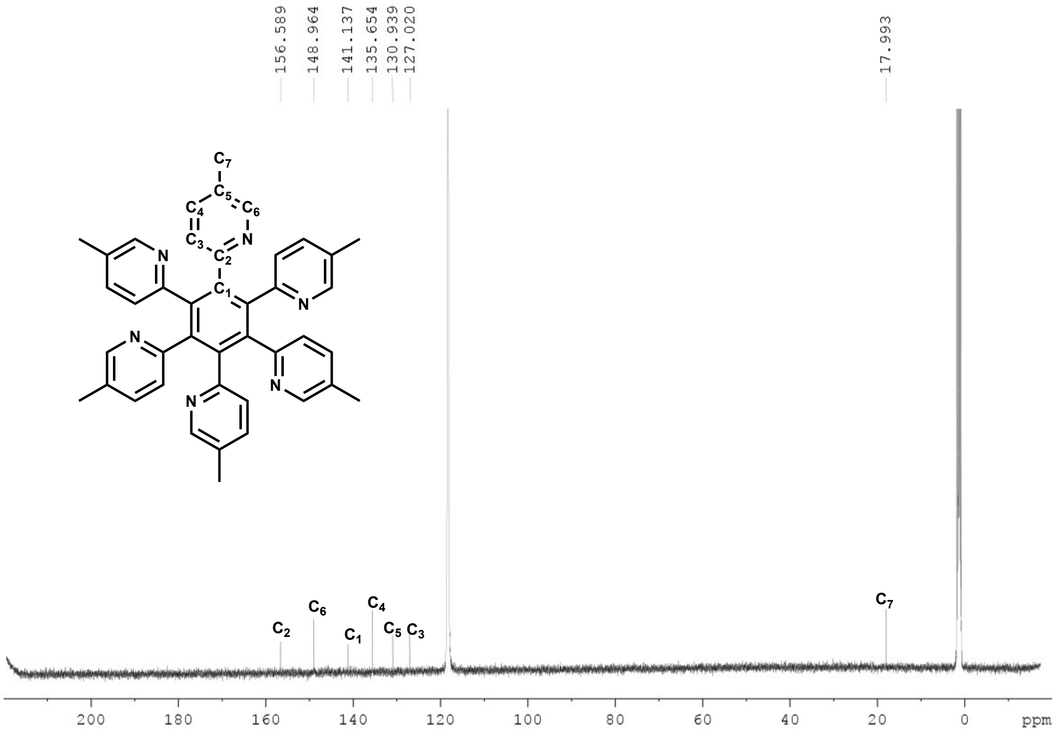

Figure S5. ^{13}C NMR spectrum of hexa(2-(5-methylpyridyl))benzene ($\mathbf{L_M}$) in CD_3CN.

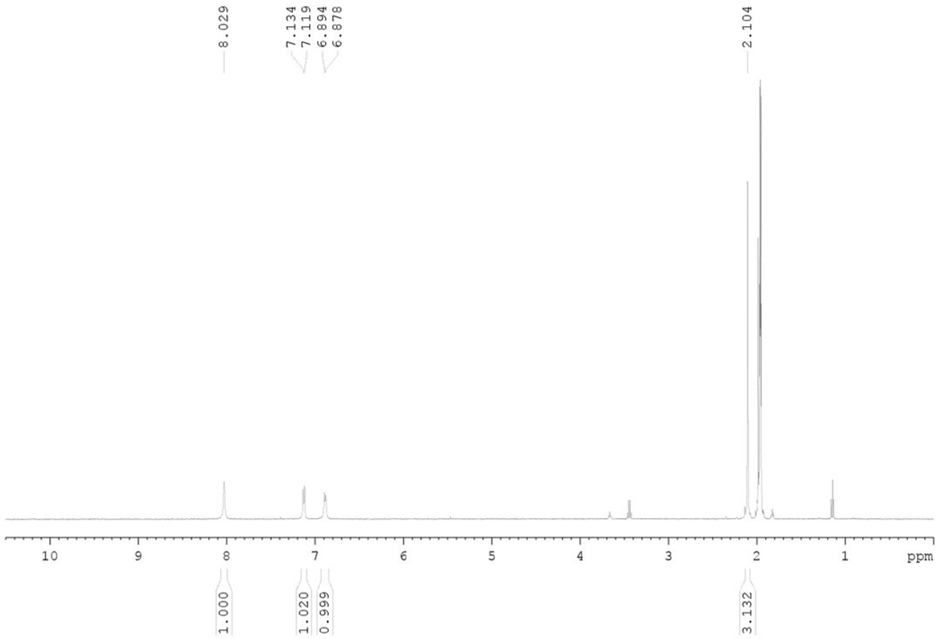

Figure S6. ^{1}H NMR spectrum of L_MCuCl(CH_3CN) (**1**) in CD_3CN at 298K.

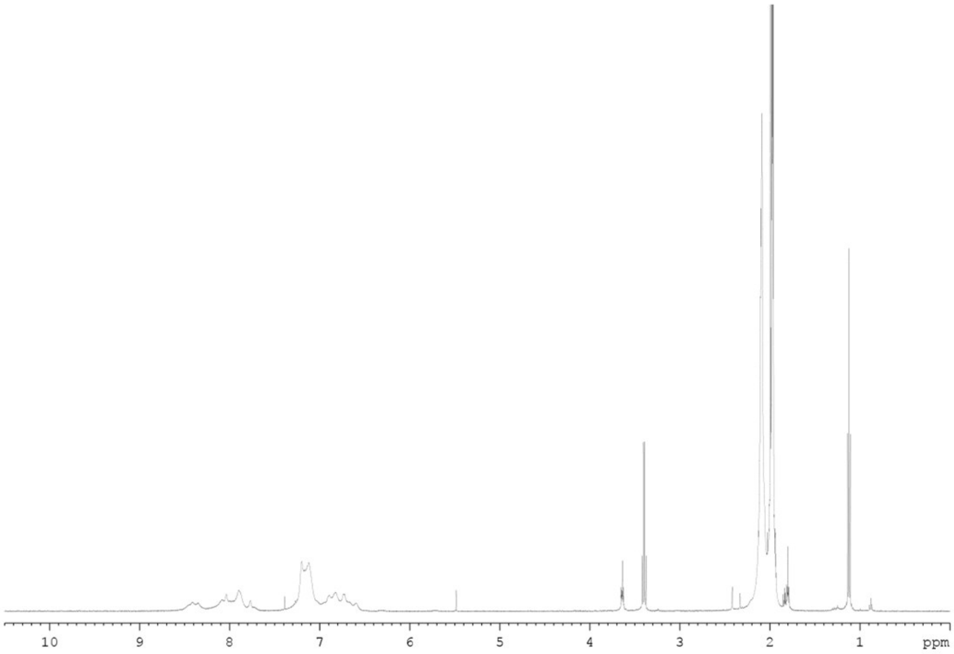

Figure S7. ^{1}H NMR spectrum of L_MCuCl(CH_3CN) (**1**) in CD_3CN at 223K.

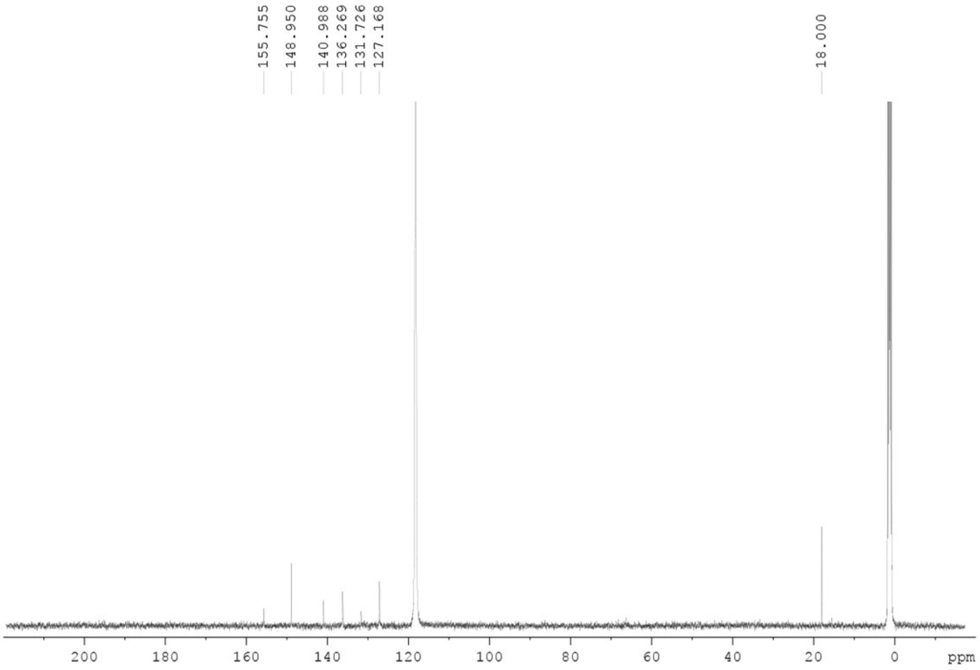

Figure S8. ^{13}C NMR spectrum of $L_MCuCl(CH_3CN)$ (**1**) in CD_3CN at 298K.

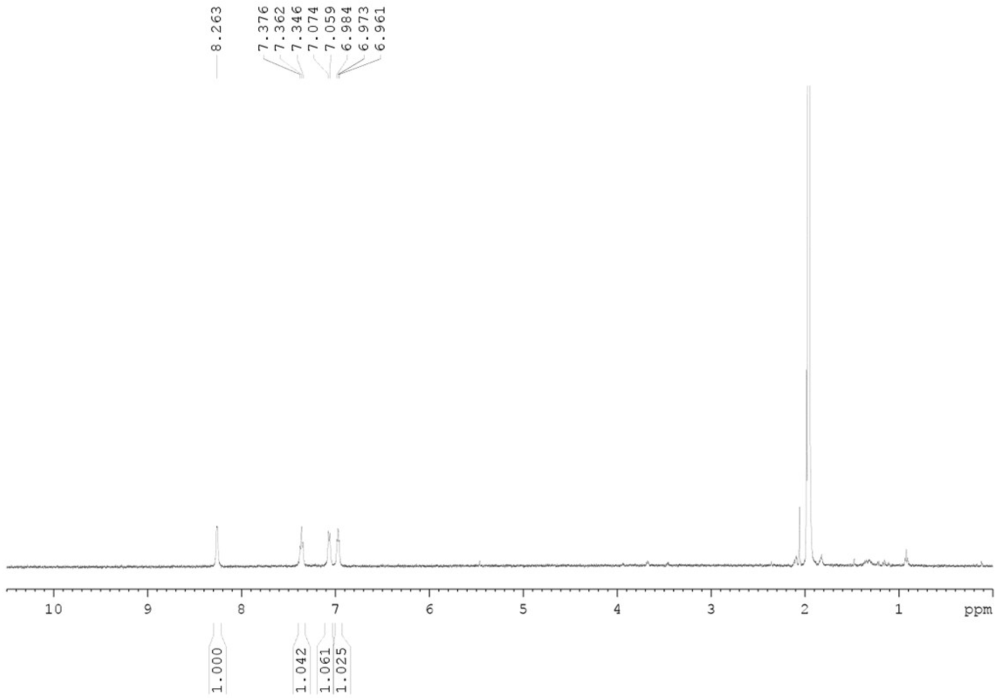

Figure S9. ^{1}H NMR spectrum of $L_HCu_2Cl_2(CH_3CN)_2$ (**2a**) in CD_3CN at 298K.

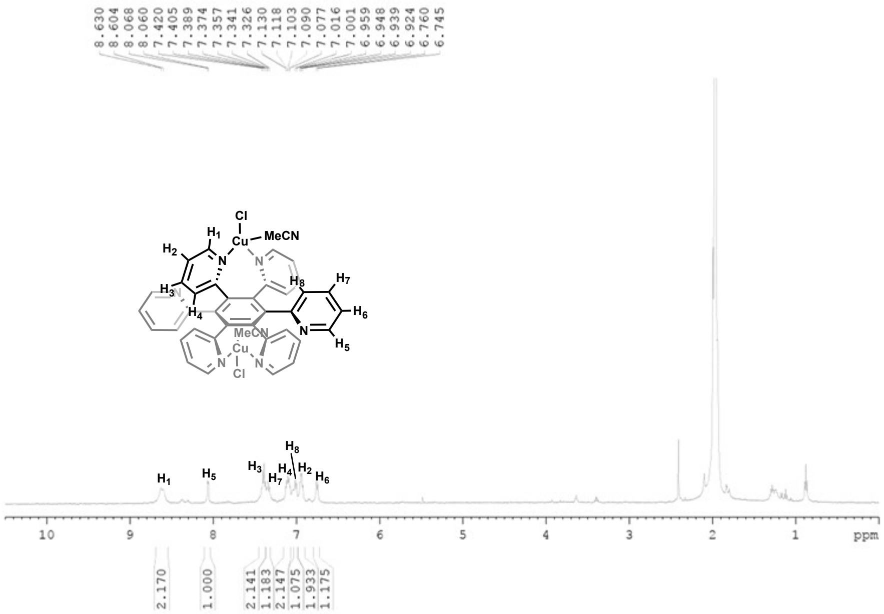

Figure S10. ^{1}H NMR spectrum of $L_HCu_2Cl_2(CH_3CN)_2$ (**2a**) in CD_3CN at 223K.

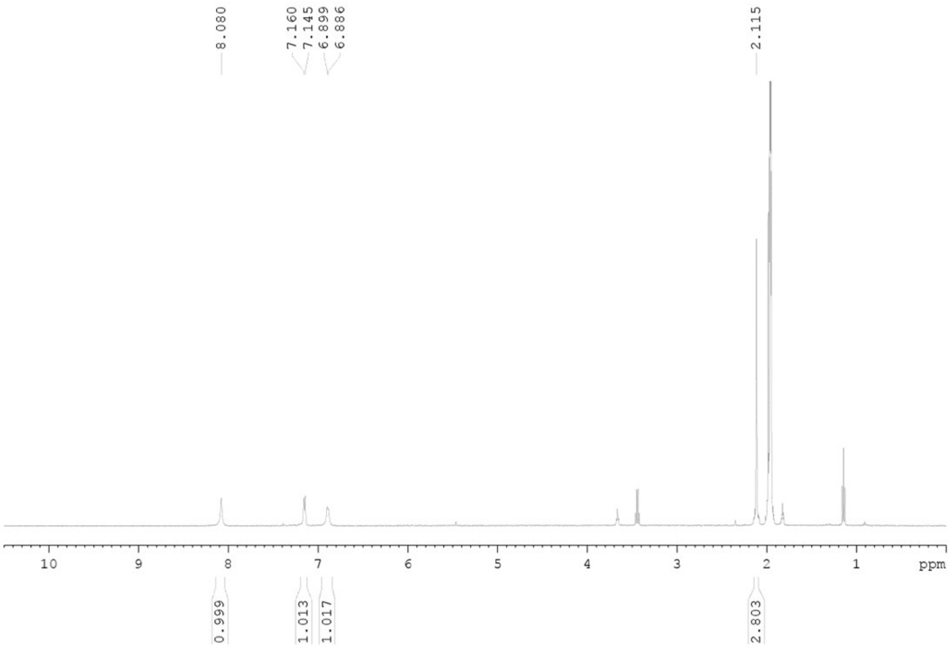

Figure S11. ^{1}H NMR spectrum of $L_MCu_2Cl_2(CH_3CN)_2$ (**2b**) in CD_3CN at 298K.

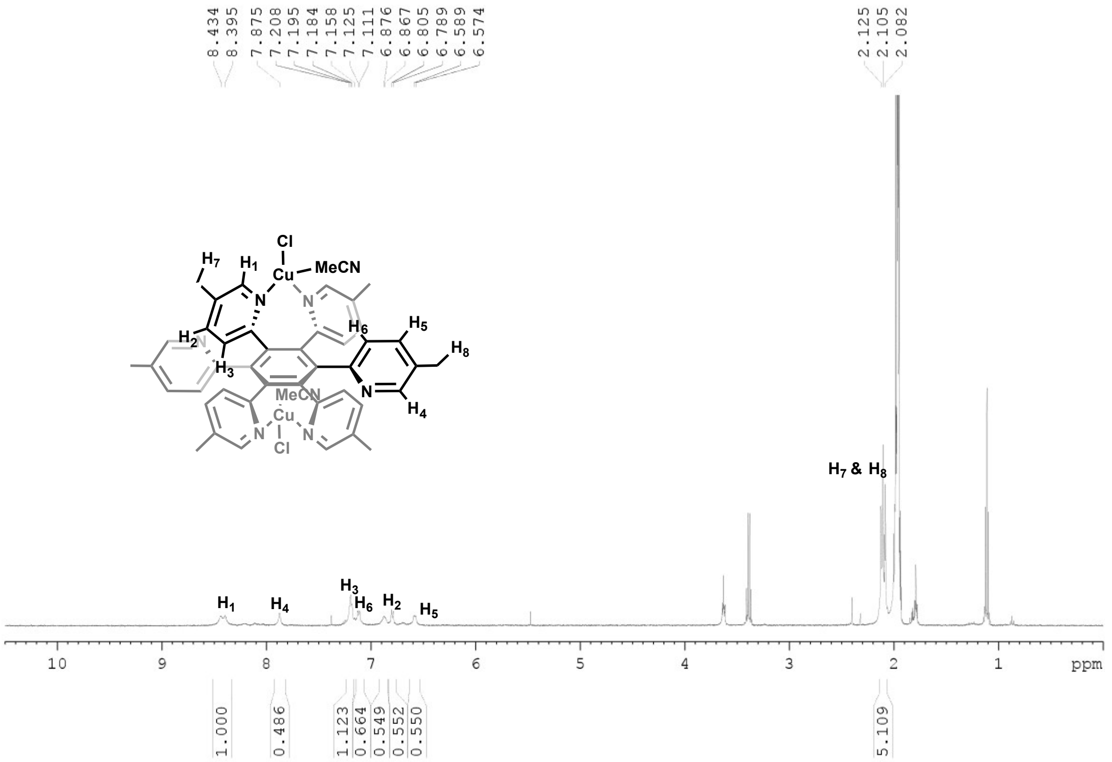

Figure S12. ^{1}H NMR spectrum of $L_MCu_2Cl_2(CH_3CN)_2$ (**2b**) in CD_3CN at 223K.

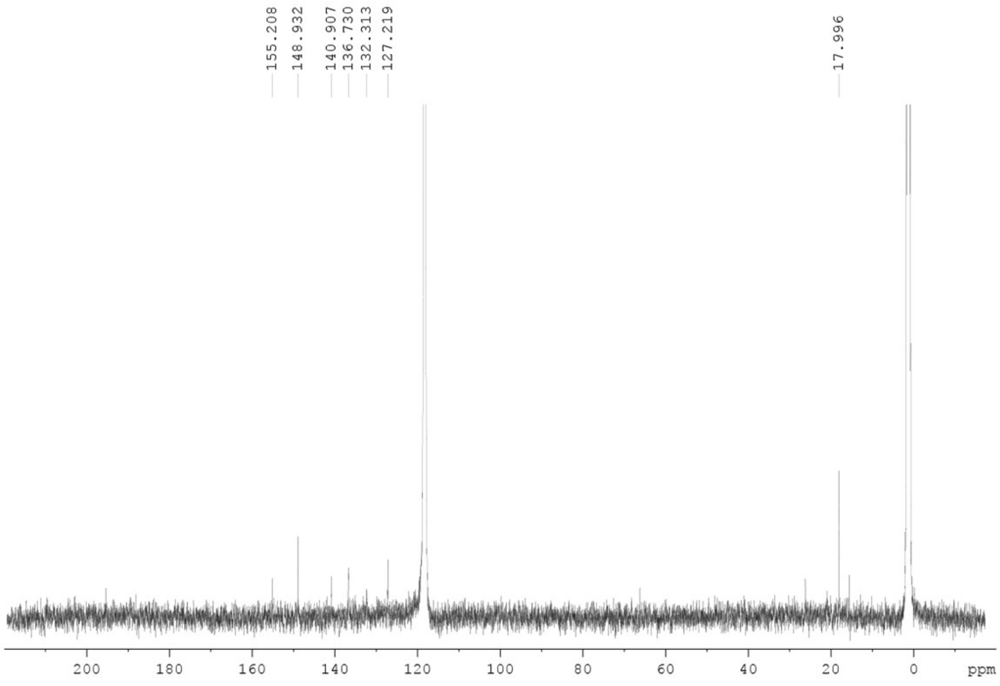

Figure S13. ^{13}C NMR spectrum of $L_MCu_2Cl_2(CH_3CN)_2$ (**2b**) in CD_3CN at 298K.

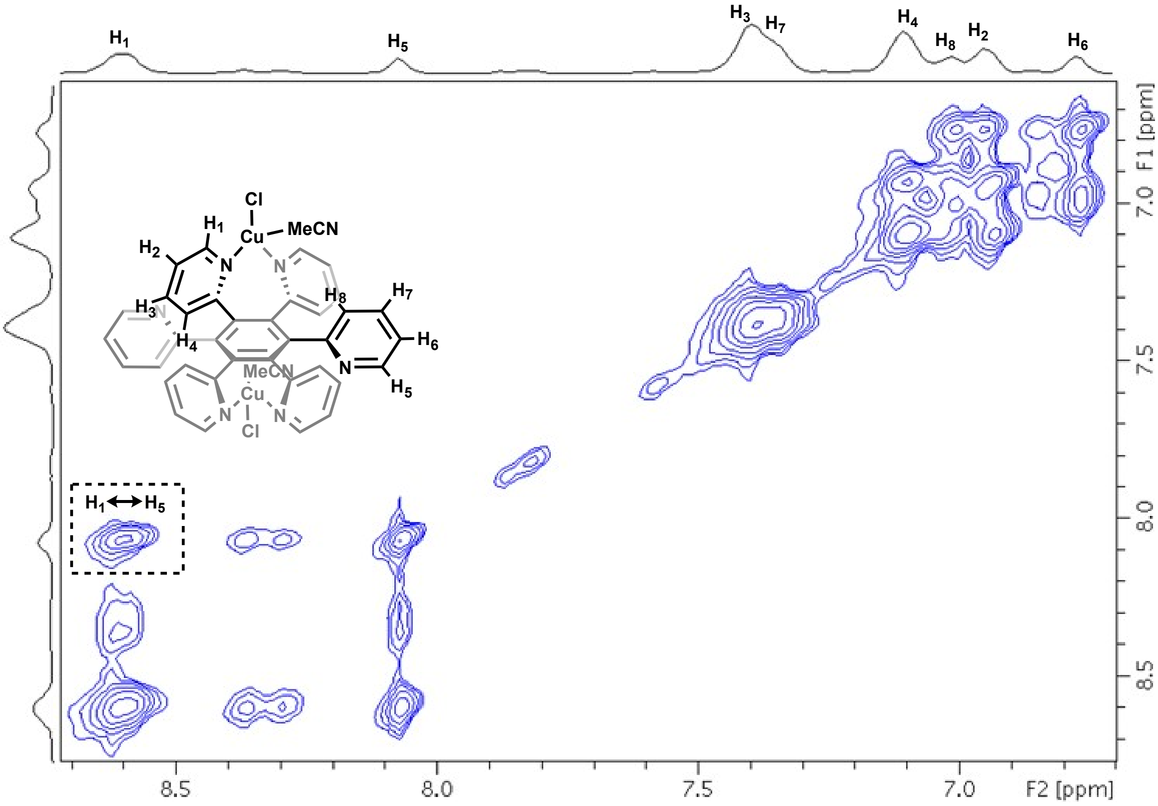

Figure S14. ^{1}H 2D EXSY of complex **2a** in CD_3CN at 233K. (τ = 0.3 sec)

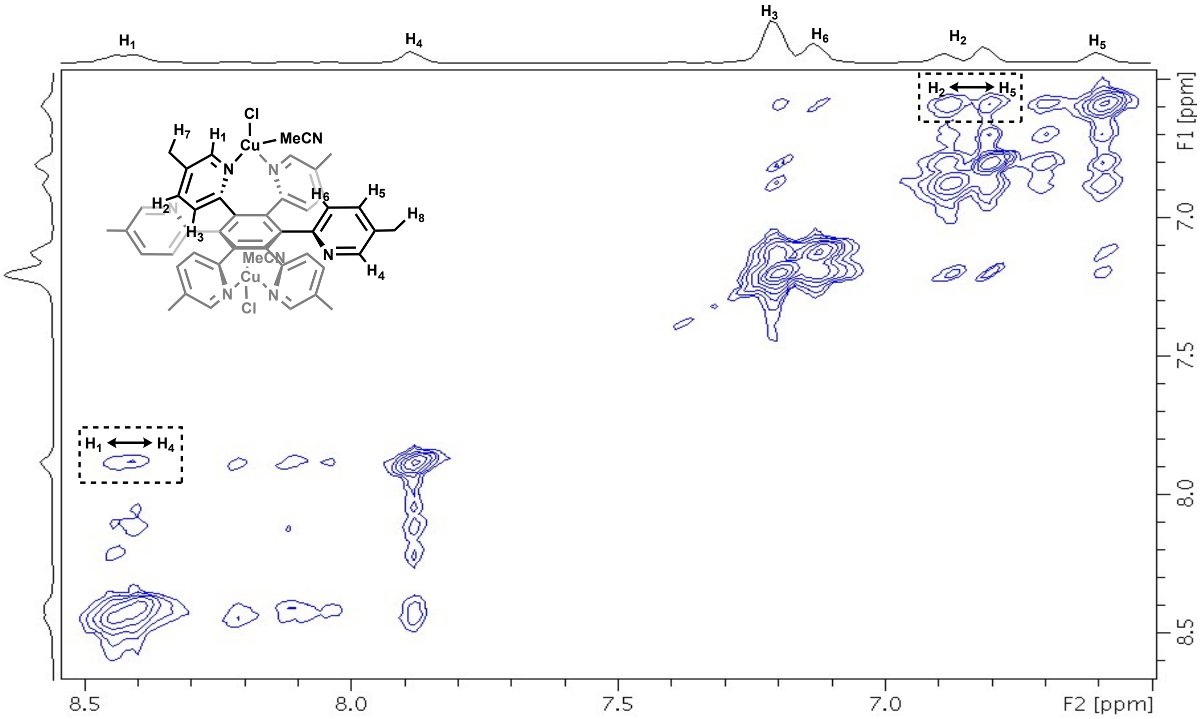

Figure S15. ^{1}H 2D EXSY of complex **2b** in CD_3CN at 223K. (τ = 0.2 sec)

4. Analysis of ^{1}H NMR studies of 1 and 2b

Solution Behaviours of 2b At 298K, in the ^{1}H NMR spectra of **2b**, only three signals at 8.08, 7.15, and 6.89 ppm at the arene region and one signal at 2.11 ppm for methyl groups were observed. The coalescence of the signal was achieved at 253K. At 223K, an almost complete peak splitting was observed. In **Figure S16**, all signals at the arene region are consistent with the structure obtained from single crystal x-ray diffraction (H_n^b for the protons in pyridine binding with copper and H_n^n for the protons in non-coordinating pyridine, n = 1 - 3). The peak splitting in H_1^b and H_3^b can be explained by different moieties given by the non-coordinating pyridine. In **Figure S15**, we can observe the cross peaks between H_1^b-H_1^n, H_2^b-H_2^n, and H_3^b-H_3^n. Also, cross peaks between the major peaks and the peaks of the intermediate are observed as well. From the 1D and 2D ^{1}H NMR spectra of **2b**, it is obvious that complex **2b** remains in the solution as a major compound and there is an intermediate in the course of dynamic process.

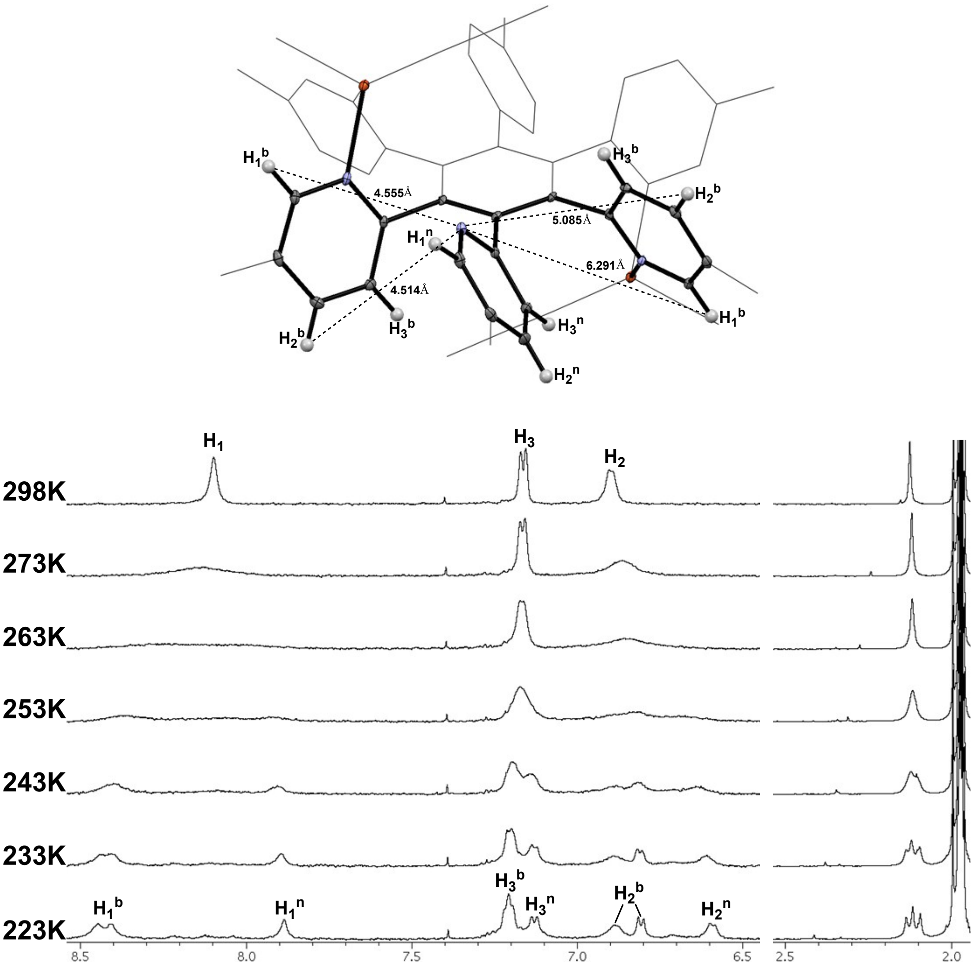

Figure S16. ^{1}H VT-NMR spectra of complex **2b** in CD_3CN.

At 298K, in the ^{1}H NMR spectra of **1**, only three signals at 8.03, 7.13 and 6.88 ppm at arene region and one signal at 2.10 ppm for methyl groups were observed. These signals are shifted to the upfield compare to the signals of **2b** and downfield compare to the signals of the ligand. In **Figure S17**, the coalescence of the signal was achieved around 233K. At 223K, the peak splitting was not completed showing different pattern compare to **2b**. Further analysis was unsuccessful due to poor resolution. Nevertheless, it is obvious that complex **1** remains in the solution in a distinctive relation to **2b**.

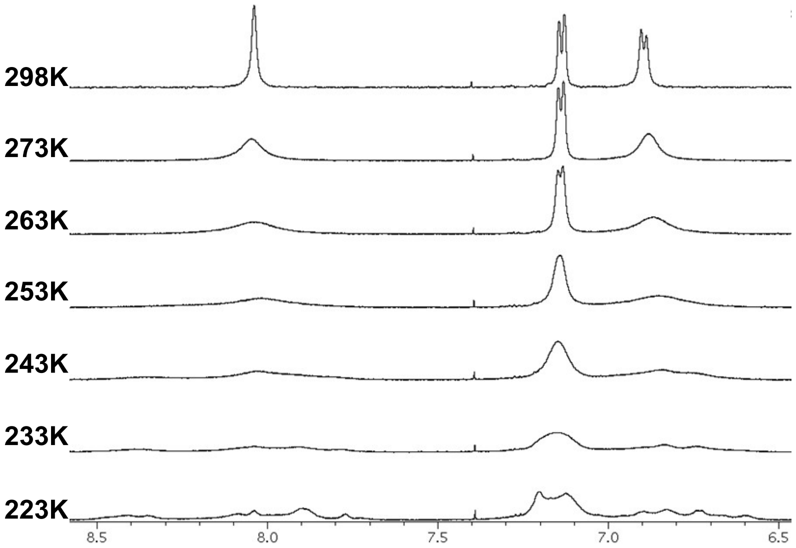

Figure S17. ^{1}H VT-NMR spectra of complex **1** in CD_3CN.

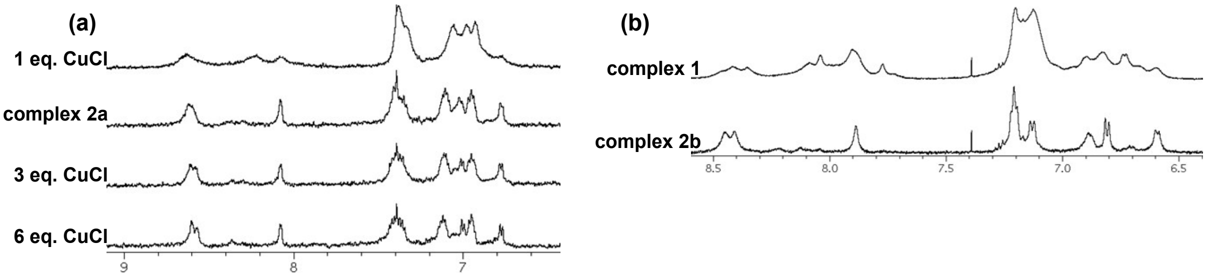

Figure S18. (a) ^{1}H NMR spectra of the solution of the complex **2a** and the solutions with 1, 3, 6 equivalent of CuCl in the CD_3CN solution at 233K. (b) ^{1}H NMR spectra of the CD_3CN solution of the complex **1** and **2b** at 233K.

5. Rate constant calculations and Erying plot of a dynamic behaviour of 2a

Since the 1st signal at 8.3 ppm didn't fully merged in a practicable temperature range, It was unfeasible to measure a rate constant of each sample by a line shape analysis. Instead, the rate constants at a specific temperature was measured from ^{1}H 2D EXSY. The rate constants, k_{obs}, can be deduced from the spectrum according to the following equation :

$$\mathbf{M} = \exp(\mathbf{R}t_{\mathrm{m}})\mathbf{M_0} \qquad [1]$$

Where **M** is a matrix whose components are the integrated intensity of the signals in 2D EXSY spectra, $\mathbf{M_0}$ is a diagonal matrix representing the EXSY spectra acquired with a mixing time (t_{m}) of zero, can be alternatively obtained from the signal intensities of 1D spectrum of the fully relaxed system. A matrix **R** is our aim of the calculation to derive exchange and relaxation rate constants.

For the case without cross relaxation, **R** has the form

$$\mathbf{R} = \begin{bmatrix} -\frac{1}{T_{11}} - k_{12} - \dots - k_{1n} & k_{12} & \dots & k_{1n} \\ k_{21} & -\frac{1}{T_{12}} - k_{21} - \dots - k_{2n} & \dots & k_{2n} \\ \dots & \dots & \dots & \dots \\ k_{n1} & k_{n2} & \dots & -\frac{1}{T_{1n}} - k_{n1} - \dots - k_{nn} \end{bmatrix} \qquad [2]$$

The kinetic constant for this motion is deduced from the H_1-H_5 signal in 2D EXSY because the signals of this hydrogen atom show large separation and are simpler than other signals to integrate.

T (K)	k_1 (s^{-1})	k_{-1} (s^{-1})
223	0.22	0.52
228	0.54	1.33
233	1.30	2.93
238	2.62	5.47
243	4.99	8.90

Table S1. The calculated rate constant of the exchange process of **2a** in CD_3CN (500 μM).

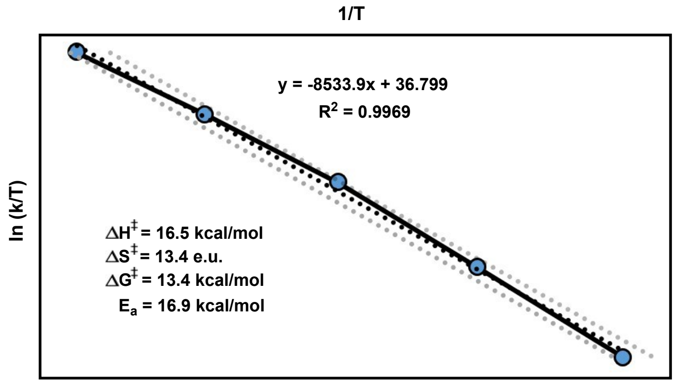

Figure S19. Eyring plot analysis and thermodynamic parameters of the exchange process of **2a** in CD_3CN (500 μM). The upper and lower lines represent the error bands of the linear regression with a 95% confidence level.

6. Photoluminescence spectra of 3, 4 and 5

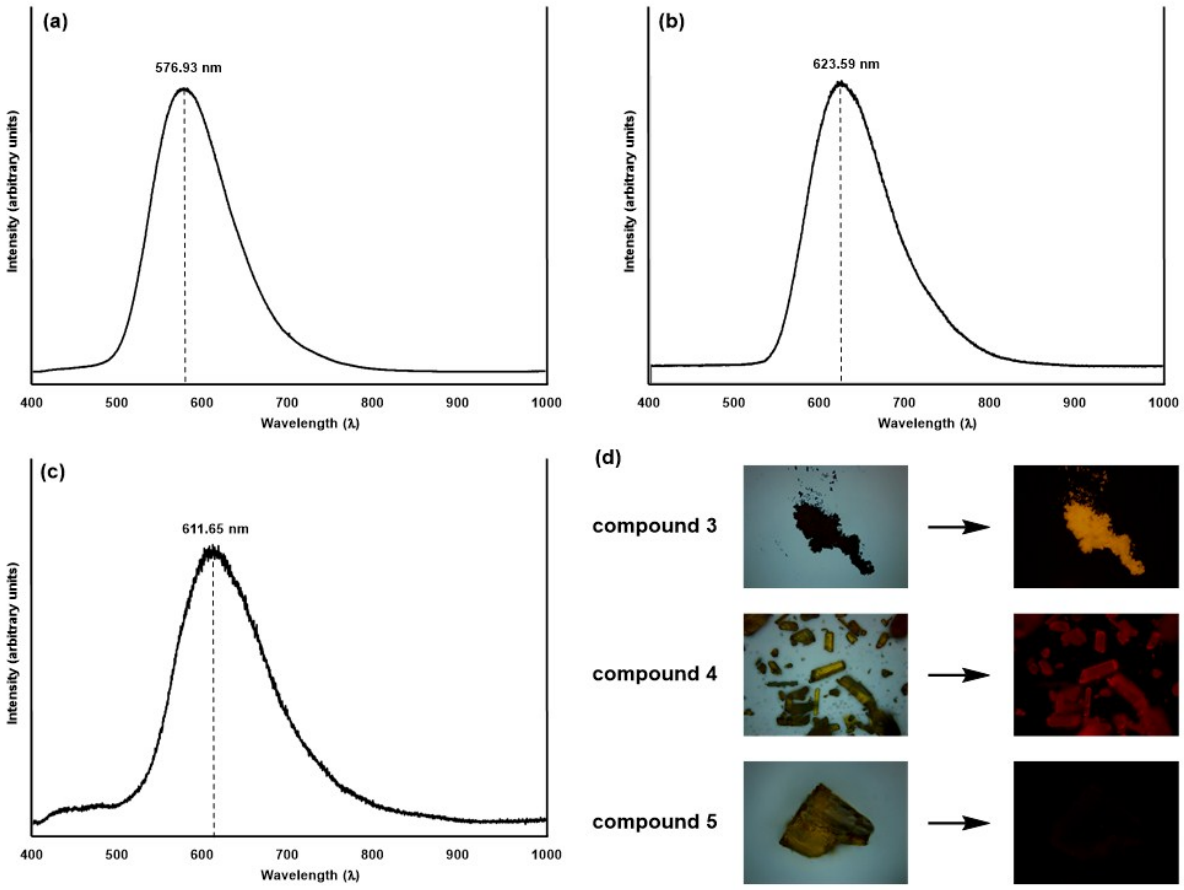

Figure S20. Solid state emission spectra of **3** (a), **4** (b) and **5** (c). (λ_{exc} = 380 nm) Optical and luminescence photographs of **3**, **4** and **5** (d).

6. Structural Analysis by X-ray Crystallography

CCDC 1828474, 1552119, 1828475, 1828476, 1828477, and 1828478 contains the supplementary crystallographic data for **1**, **2a**, **2b**, **3**, **4** and **5** respectively. These data can be obtained free of charge via www.ccdc.cam.ac.uk/cgibin/catreq.cgi (or from the Cambridge Crystallographic Data Centre, 12, Union Road, Cambridge CD21EZ, UK; fax (+44) 1223-336-033; or deposit@ccdc.cam.ac.uk). For all six compounds, all the non-hydrogen atoms were refined anisotropically and hydrogen atoms were added to their ideal positions.

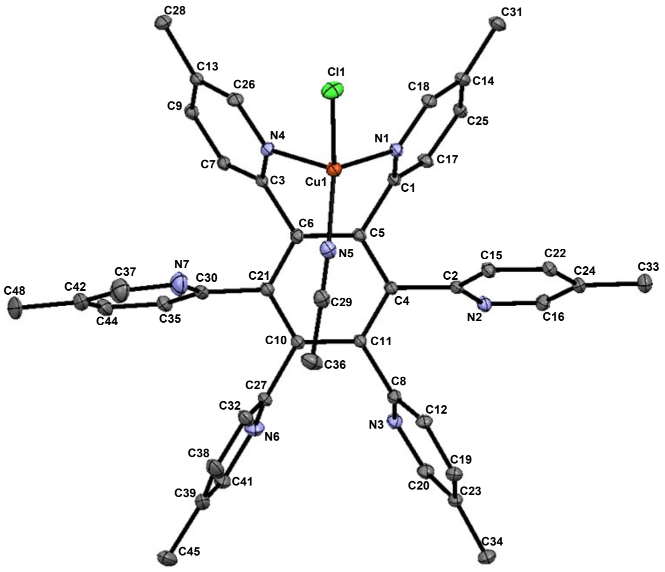

Figure S21. ORTEP diagram of $L_MCuCl(CH_3CN)$ (**1**), Ellipsoids are shown at 25% probability level.

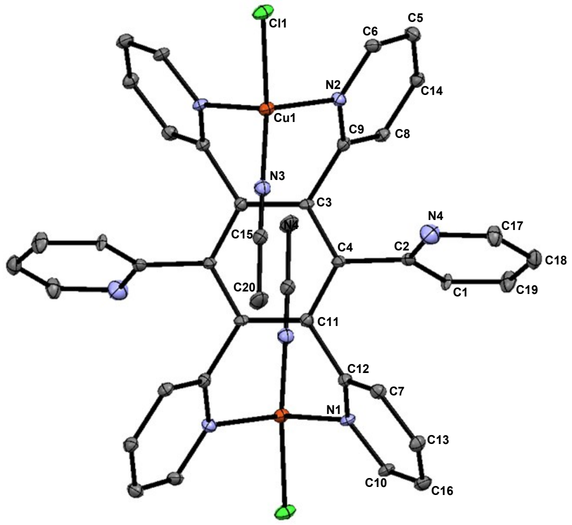

Figure S22. ORTEP diagram of $L_HCu_2Cl_2(CH_3CN)_2$ (**2a**), Ellipsoids are shown at 50% probability level.

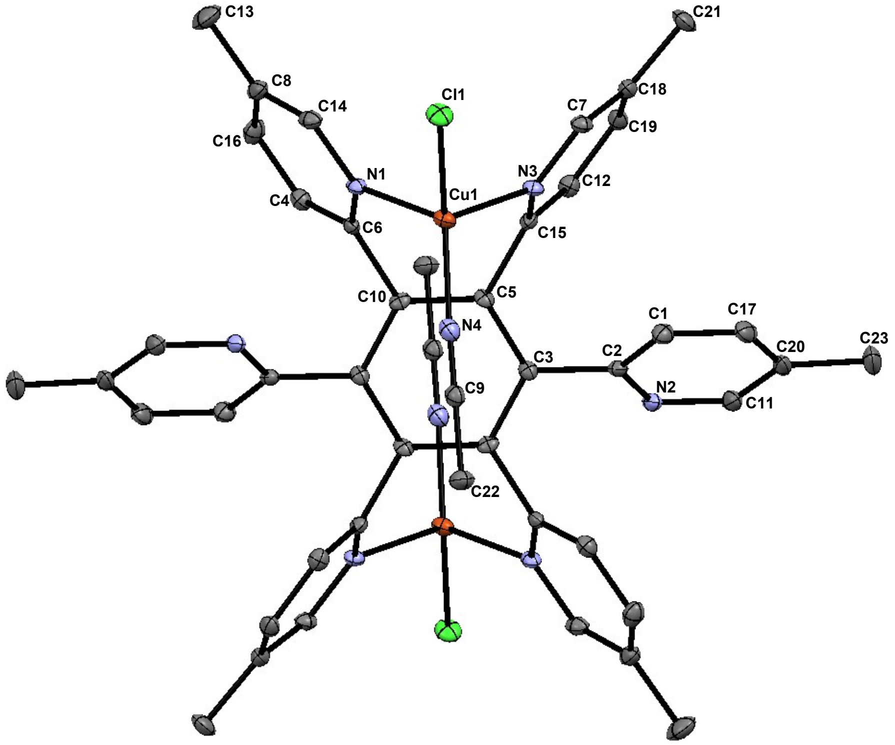

Figure S23. ORTEP diagram of $L_MCu_2Cl_2(CH_3CN)_2$ (**2b**), Ellipsoids are shown at 50% probability level.

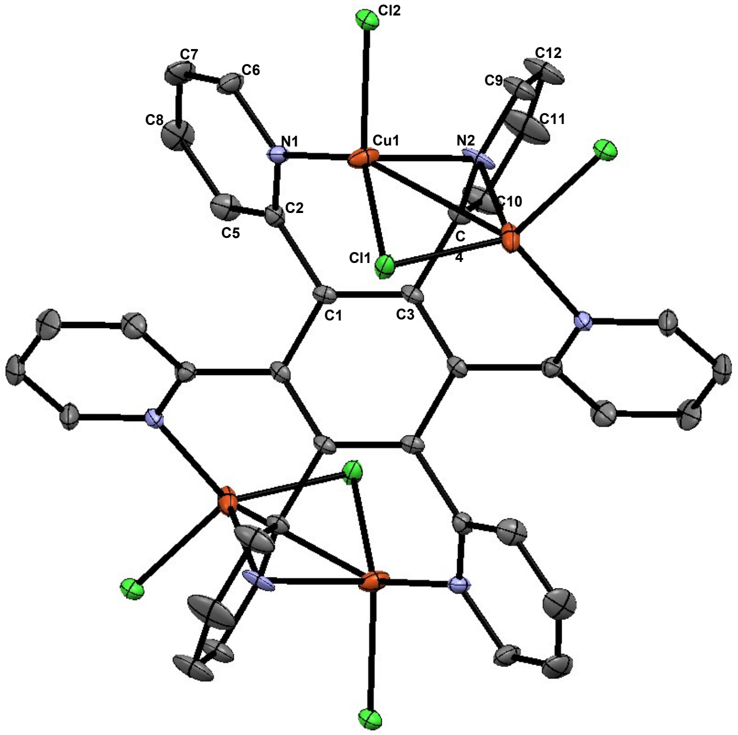

Figure S24. ORTEP diagram of $[L_HCu_4Cl_4]_n$ (**3**), Ellipsoids are shown at 50% probability level.

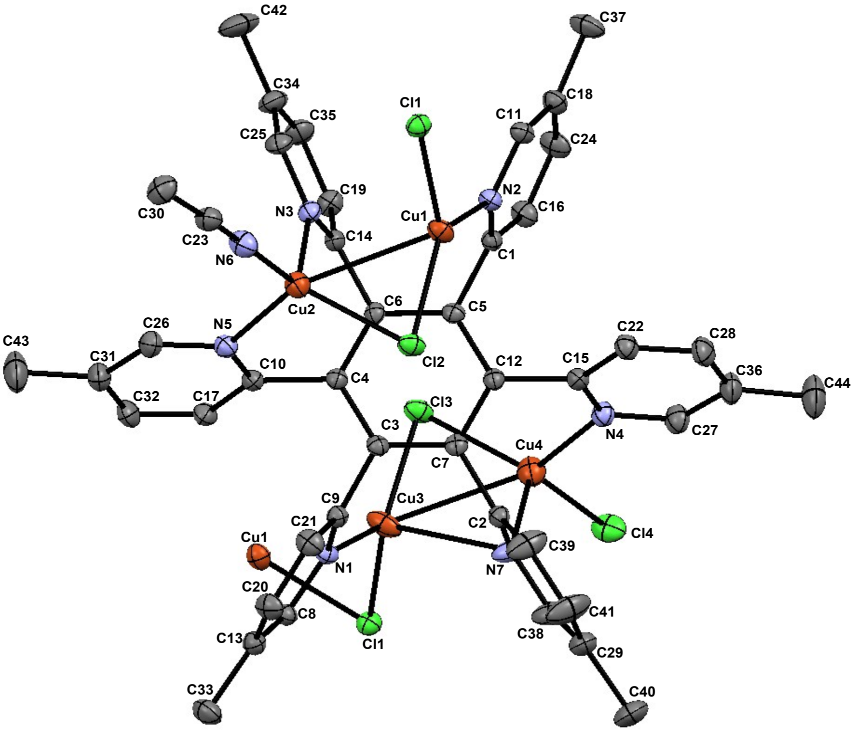

Figure S25. ORTEP diagram of $[L_MCu_4Cl_4(CH_3CN)]_n{\cdot}(CH_3CN)_n$ (**4**), Ellipsoids are shown at 25% probability level.

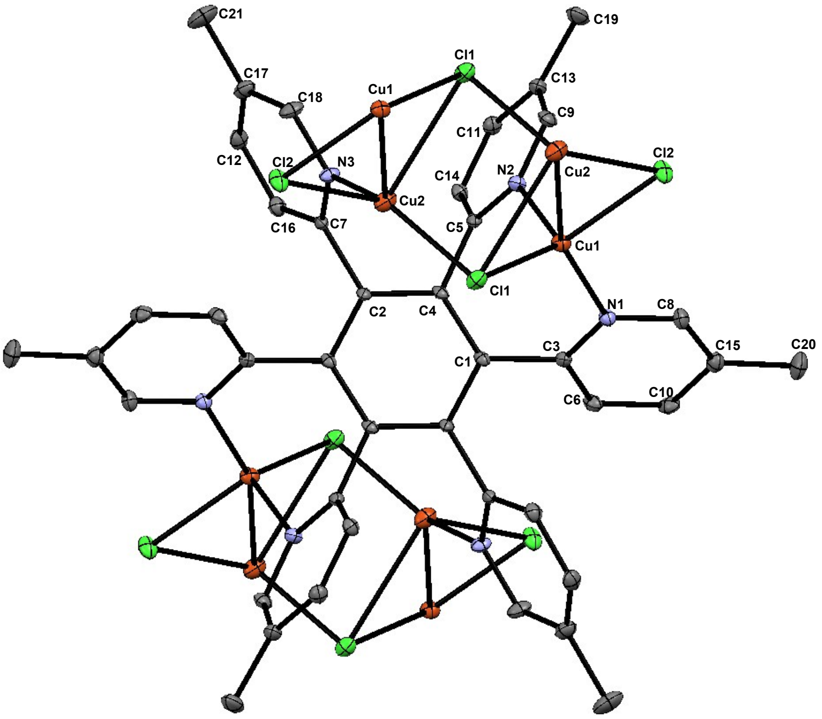

Figure S26. ORTEP diagram of $[L_MCu_4Cl_4]_n{\cdot}(THF)_n$ (**5**), Ellipsoids are shown at 50% probability level.

Crystal data information of **5** (output.cif)

_cell.length_a 9.465

_cell.length_b 14.559

_cell.length_c 17.362

_cell.angle_alpha 90.000

_cell.angle_beta 95.379

_cell.angle_gamma 90.000

_cell.length_a_esd 0.002

_cell.length_b_esd 0.002

_cell.length_c_esd 0.002

_cell.angle_alpha_esd 0.0

_cell.angle_beta_esd 0.002

_cell.angle_gamma_esd 0.0

_cell.volume 2382.0

_diffrn_radiation.wavelength 0.70000

_diffrn_measurement.method '\w scans'

_diffrn_measurement.details

' 1.00 degrees, 1.00 sec, detector distance 63.00 mm'

_reflns.observed_criterion_sigma_I -3

_reflns.observed_criterion_sigma_F 0

_reflns.d_resolution_low 50.00

_reflns.d_resolution_high 0.71

_reflns.number_obs 30745

```
_reflns.number_all 30745
_reflns.number_unique 7083
_reflns.percent_possible_obs 97.9
_reflns.pdbx_Rmerge_I_obs 0.043
_reflns.pdbx_Rsym_value 0.043
_reflns.pdbx_I_obs 916.6
_reflns.pdbx_sigmaI 23.6
_reflns.pdbx_netI_over_av_sigmaI 38.839
_reflns.pdbx_redundancy 4.3
_reflns_shell.d_res_high 0.71
_reflns_shell.d_res_low 0.72
_reflns_shell.percent_possible_all 94.2
_reflns_shell.Rmerge_I_obs 0.072
_reflns_shell.pdbx_Rsym_value 0.072
_reflns_shell.pdbx_I_obs 274.6
_reflns_shell.pdbx_sigmaI 17.2
_reflns_shell.meanI_over_sigI_obs 15.965
_reflns_shell.pdbx_redundancy 4.1
_reflns_shell.cc12 0.994
_diffrn_reflns.av_R_equivalents 0.043
_diffrn_reflns.number 30745
_cell_measurement.reflns_used 30745
```

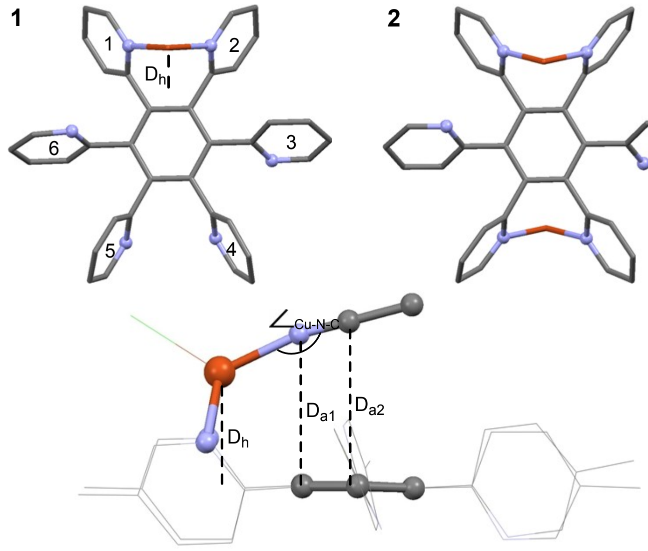

	D_h	D_{a1}	D_{a2}	$\angle_{Cu\text{-}N\text{-}C}$	$\angle_1$	$\angle_2$	$\angle_3$	$\angle_4$	$\angle_5$	$\angle_6$	$\angle_{av}$
1	2.422	3.277	3.576	168.79	63.68	66.15	63.10	75.27	76.67	72.54	69.57
2a	2.422	3.321	3.722	175.31	70.31	71.31	65.82	70.31	71.31	65.82	69.14
2b	2.545	3.365	3.796	176.59	65.89	74.17	55.42	65.89	74.17	55.42	65.16

* D_h : Height of the copper atom from the plane of the central benzene(▯)
* D_{a1} : Distance between the plane of the central arene and the nitrogen in acetonitrile(▯)
* D_{a2} : Distance between the plane of the central arene and the sp^3 carbon in acetonitrile(▯)
* $\angle_{Cu\text{-}N\text{-}C}$: angle between Cu-sp^3 N-sp^3 C(°)
* $\angle_n$: angle between the plane of nth pyridine and the plane of central benzene(°)
* $\angle_{av}$: average angle of $\angle_1$ - $\angle_6$(°)

Figure S27. Detailed informations about angles and distances of **1**, **2a** and **2b**.

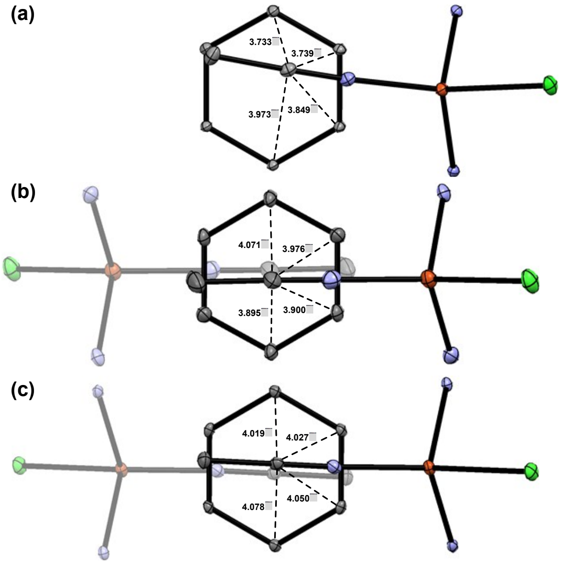

Figure S28. Detailed informations about the distances between sp carbon in acetonitrile and carbons in central arene in **1 (a)**, **2a (b)** and **2b (c)**.

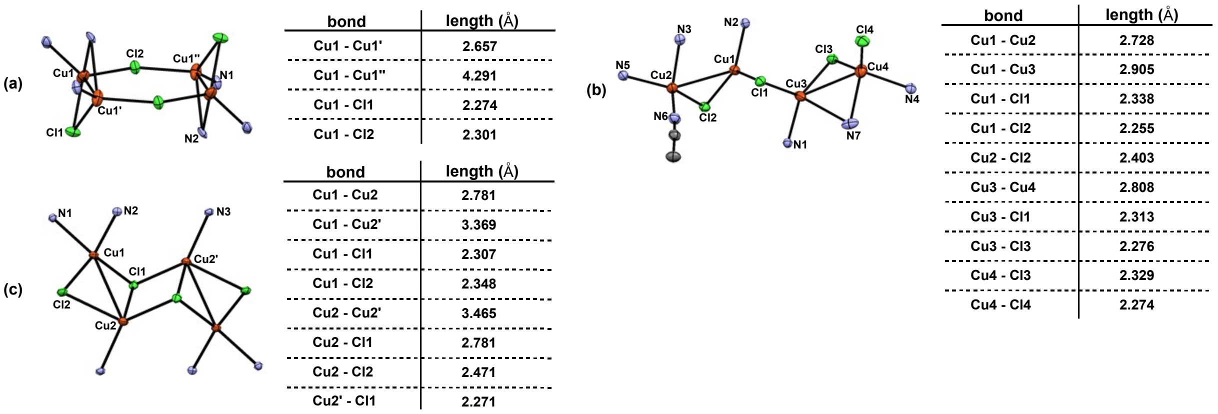

(a)

bond	length (Å)
Cu1 - Cu1'	2.657
Cu1 - Cu1''	4.291
Cu1 - Cl1	2.274
Cu1 - Cl2	2.301

(b)

bond	length (Å)
Cu1 - Cu2	2.728
Cu1 - Cu3	2.905
Cu1 - Cl1	2.338
Cu1 - Cl2	2.255
Cu2 - Cl2	2.403
Cu3 - Cu4	2.808
Cu3 - Cl1	2.313
Cu3 - Cl3	2.276
Cu4 - Cl3	2.329
Cu4 - Cl4	2.274

(c)

bond	length (Å)
Cu1 - Cu2	2.781
Cu1 - Cu2'	3.369
Cu1 - Cl1	2.307
Cu1 - Cl2	2.348
Cu2 - Cu2'	3.465
Cu2 - Cl1	2.781
Cu2 - Cl2	2.471
Cu2' - Cl1	2.271

Figure S29. Detailed information about the distances between atoms in Cu_4Cl_4 clusters of **3** (a), **4** (b) and **5** (c).

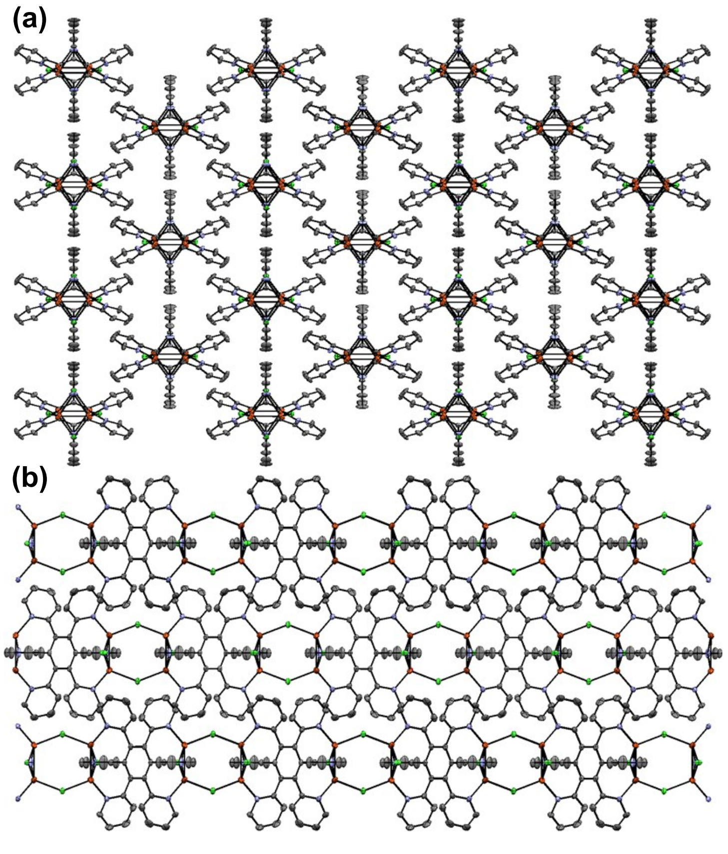

Figure S30. Perspective view for the packing structure of $[L_HCu_4Cl_4]_n$ (**3**), Ellipsoids are shown at 50% probability level.

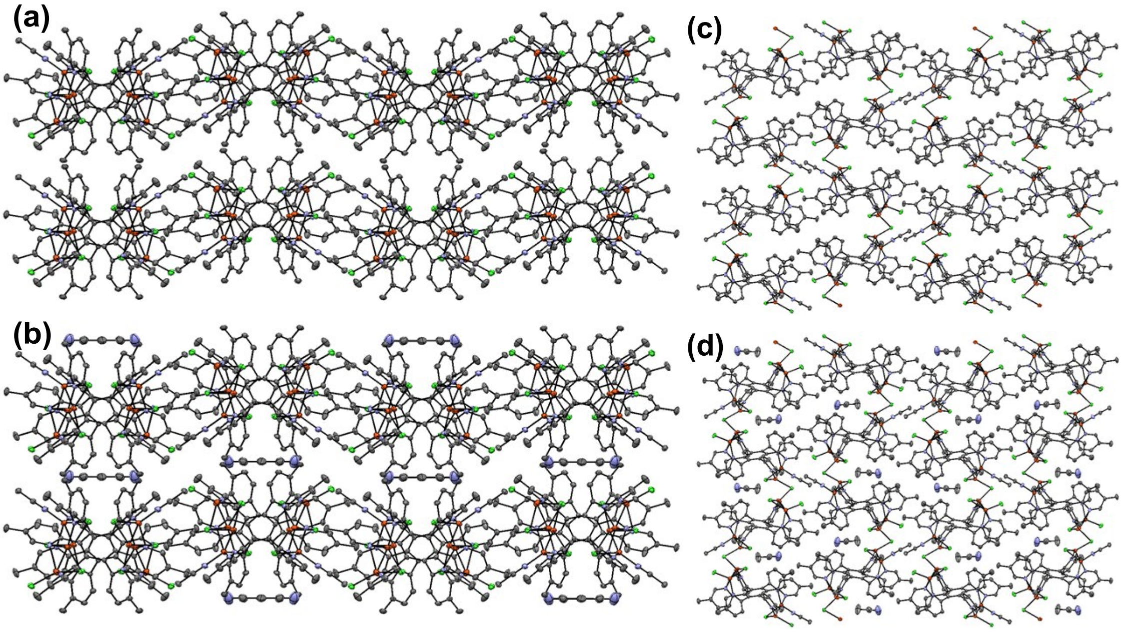

Figure S31. Perspective view for the packing structure of $[L_MCu_4Cl_4(CH_3CN)]_n{\cdot}(CH_3CN)_n$ (**4**), Ellipsoids are shown at 50% probability level. The lattice solvent molecules are omitted in (a) and (c).

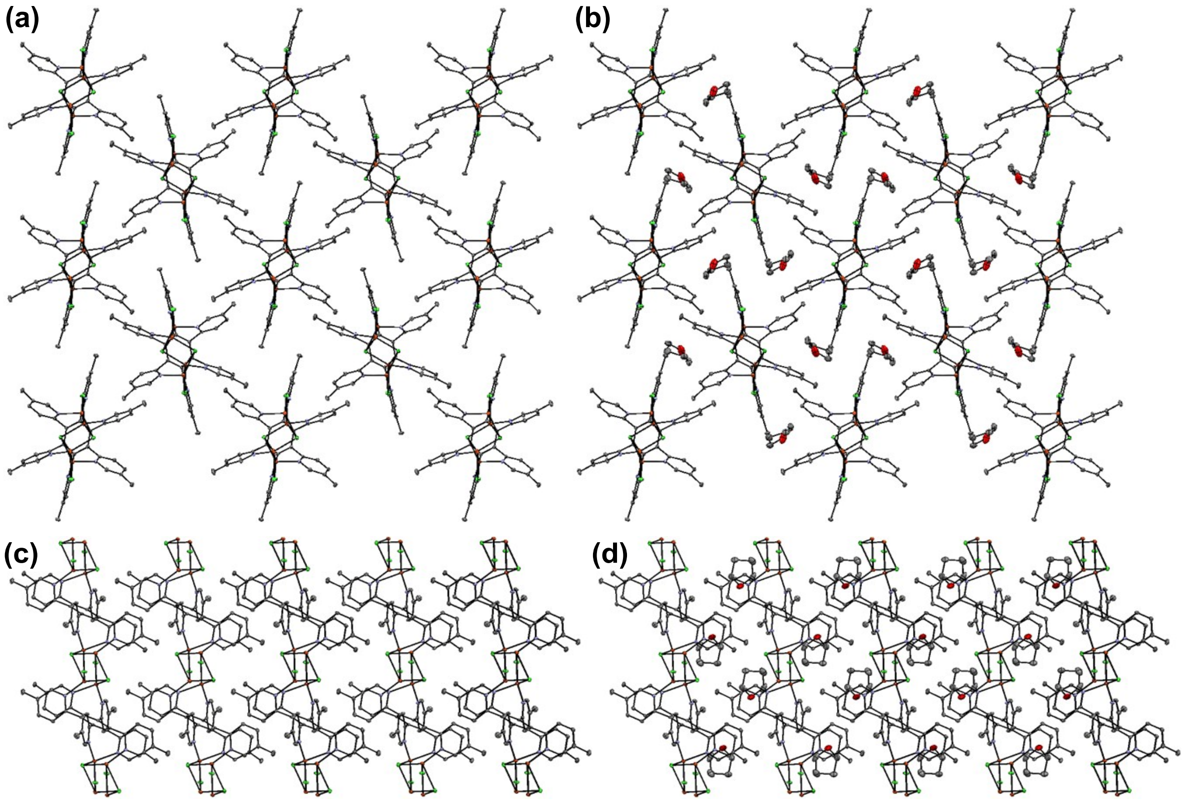

Figure S32. Perspective view for the packing structure of $[L_MCu_4Cl_4]_n{\cdot}(THF)_n$ (**5**), Ellipsoids are shown at 50% probability level. The lattice solvent molecules are omitted in (a) and (c).

Reference

(1) Chun Liu, N. H., Xiaoxiao Song, Jieshan Qiu A General and Highly Efficient Method for the Construction of Aryl-Substituted N-Hereoarenes. *Eur. J. Org. Chem.* **2010**, *2010*, 4.

(2) Scrase, T. G.; O'Neill, M. J.; Peel, A. J.; Senior, P. W.; Matthews, P. D.; Shi, H. Y.; Boss, S. R.; Barker, P. D. Selective Lability of Ruthenium(II) Arene Amino Acid Complexes. *Inorg. Chem.* **2015**, *54*, 3118.

(3) Dolomanov, O. V.; Bourhis, L. J.; Gildea, R. J.; Howard, J. A. K.; Puschmann, H. OLEX2: a complete structure solution, refinement and analysis program. *J. Appl. Cryst.* **2009**, *42*, 339.

(4) Millan, C.; Sammito, M.; Garcia-Ferrer, I.; Goulas, T.; Sheldrick, G. M.; Uson, I. Combining phase information in reciprocal space for molecular replacement with partial models. *Acta Crys. D* **2015**, *71*, 1931.

(5) Sheldrick, G. M. SHELXT - Integrated space-group and crystal-structure determination *Acta Cryst. A* **2015**, *71*, 3-8.